THE COMA OF COMET 9P/TEMPEL 1

C. M. LISSE[1,2,*], M. F. A'HEARN[2], T. L. FARNHAM[2], O. GROUSSIN[2], K. J. MEECH[3], U. FINK[4] and D. G. SCHLEICHER[5]

[1]*Planetary Exploration Group, Space Department, Johns Hopkins University Applied Physics Laboratory, 11100 Johns Hopkins Road, Laurel, MD 20723, U.S.A.*

[2]*Department of Astronomy, University of Maryland, College Park, MD 20742, U.S.A.*

[3]*Institute for Astronomy, University of Hawaii, 2680 Woodlawn Drive, Honolulu, HI 96822, U.S.A.*

[4]*Department of Planetary Sciences, University of Arizona, LPL, Tucson, AZ 85721, U.S.A.*

[5]*Lowell Observatory, 1400 West Mars Hill Road, Flagstaff, AZ 86001, U.S.A.*

*(*Author for correspondence; E-mails: carey.lisse@jhuapl.edu, lisse@astro.umd.edu)*

(Received 13 September 2004; Accepted in final form 28 December 2004)

Abstract. As comet 9P/Tempel 1 approaches the Sun in 2004–2005, a temporary atmosphere, or "coma," will form, composed of molecules and dust expelled from the nucleus as its component icy volatiles sublimate. Driven mainly by water ice sublimation at surface temperatures $T > 200$ K, this coma is a gravitationally unbound atmosphere in free adiabatic expansion. Near the nucleus ($\leq 10^2$ km), it is in collisional equilibrium, at larger distances ($\geq 10^4$ km) it is in free molecular flow. Ultimately the coma components are swept into the comet's plasma and dust tails or simply dissipate into interplanetary space. Clues to the nature of the cometary nucleus are contained in the chemistry and physics of the coma, as well as with its variability with time, orbital position, and heliocentric distance.

The DI instrument payload includes CCD cameras with broadband filters covering the optical spectrum, allowing for sensitive measurement of dust in the comet's coma, and a number of narrowband filters for studying the spatial distribution of several gas species. DI also carries the first near-infrared spectrometer to a comet flyby since the VEGA mission to Halley in 1986. This spectrograph will allow detection of gas emission lines from the coma in unprecedented detail. Here we discuss the current state of understanding of the 9P/Tempel 1 coma, our expectations for the measurements DI will obtain, and the predicted hazards that the coma presents for the spacecraft.

Keywords: comets, coma, dust, gas, composition, jets, 9P/Tempel 1, Deep Impact

Introduction

The coma of comet 9P/Tempel 1 is of interest to the Deep Impact (DI) mission as a phenomenon itself, as a component of the measured flux in the DI images, and as an obstacle that the DI spacecraft must traverse. More importantly, however, the coma represents the end product, and thus the measurable entity, of the material excavated during the impact. The coma is also the primary characteristic seen in ground-based observations, and is thus important for revealing the long-term changes that result from the impact, as well as for providing comparisons to other comets. We have attempted to collect and interpret all currently available information concerning the

Space Science Reviews (2005) 117: 161–192
DOI: 10.1007/s11214-005-3384-6

dust and gas emitted by 9P/Tempel 1. Because of its nearly exact 11:2 orbital commensurability with Earth, Tempel 1 alternates between favorable and unfavorable apparitions for Earth-based observing, and the state of our understanding of the coma is moderate at best. Nearly all near-perihelion data of which we are aware are from the favorable apparitions in 1983 and 1994. There are, in addition, numerous images of the dust coma, obtained as part of the Deep Impact project, from the 2000 apparition, but because this was an unfavorable apparition, all the data were obtained when the comet was far from perihelion.

It will be convenient to separate our discussion into the gaseous and dusty components of the coma. In this article, we will focus on what we believe the state of the coma will be near the time of the encounter, as this is particularly relevant to the measurements that will be made by Deep Impact. However, because the impact may produce changes in the long-term behavior of the comet, we will also discuss the properties of the coma as observed over the full range of heliocentric distances.

It is important to note that the ensuing discussion of the current knowledge of Tempel 1's coma is inherently biased. The outer regions of cometary comae, due to observability considerations, are relatively well studied (cf. in *Comets II* by Schleicher and Farnham, 2005; Bockelée-Morvan *et al.*, 2005; Feldman *et al.*, 2005; Crifo *et al.*, 2005; Boice and Huebner, 2005; Combi *et al.*, 2005). Here the density of the outflow is low enough and the mean free path between collisions is large enough that the gas is in the molecular flow regime; photochemistry of volatile species, reactions via H-atom addition, and collisional excitation and charge exchange with the solar wind dominate. Dust particles have reached a terminal velocity from the coma expansion and enter a regime where the dominant forces are solar radiation pressure and gravity. By contrast, in the innermost regions of the coma, from the nuclear surface to $\sim 10^3$ km, gas densities range upwards of 10^6 mol cm^{-3}, collisions are frequent, and the outflow is turbulent and complicated. Multi-body chemistry driven by collisions occurs in the near nucleus zone, and transient chemical species are common. Narrow jets of material are formed, though it is not clear, even after the Deep Space-1 (DS-1) and STARDUST flybys of comets Borrelly and Wild 2, whether the focusing of outflow material is due to surface and subsurface structures in the cometary nucleus or to hydrodynamic outflow behavior in the inner coma, or both. It is within this region that dust particles released by volatile sublimation are swept up and accelerated by the outflowing gas to typical terminal velocities of 1–500 m s^{-1}. Plasma species, created by photoionization of outflowing volatiles and by the in-streaming solar wind, are unable to penetrate into this region due to mass loading and magnetic field concentration. Because it is difficult to resolve from the ground, the inner coma is poorly understood and its characteristics have mostly been inferred from studies of the coma as a whole.

As discussed in the companion article by Hampton *et al.* (this volume), the cameras on Deep Impact include seven intermediate-band filters covering the optical

spectrum (all seven are included in the HRI filter wheel, while a subset of four are in the MRI filter wheel). These filters will allow sensitive measurements of dust in the comet's coma. The MRI also carries three narrowband filters for isolating the emission bands of CN, OH, and C_2 gaseous species. One of the most exciting potential returns of the DI mission is the possibility of chemical maps of the little-studied inner coma region at $\sim$10 m resolution. Investigating the chemistry of any jet structures that are present and tracing them back to the nucleus will greatly increase our understanding of the nature of the active regions that produce jets. The HRI near-infrared spectrometer will allow detection of emission lines from neutral gas species in the coma in unprecedented spatial and spectral detail and will also provide novel results on the size, composition and spatial variations of the coma dust. Although the spectroscopic measurements are an important part of coma studies in the DI mission, we will only summarize them here. They are discussed in detail by Sunshine *et al.* (2005) in a companion paper in this volume.

Current Knowledge of Tempel 1's Coma

In the next two sections, we discuss what is known from previous observations about the composition and structure of Tempel 1's coma. Unfortunately, the total amount of archival data is small, and much of this is unpublished, because the low-activity comet 9P/Tempel 1 is rarely bright as seen from the Earth and thus is not a favorite target of observers. Fortunately, the 2005 apparition is the next good one, so extensive ground-based observations can be obtained in support of the DI encounter.

The Gas Coma

Abundances of gaseous species are available from four independent programs – ultraviolet spectroscopy with IUE in 1983 and 1994, optical spectrophotometry at McDonald Observatory using the Image Dissector Scanner (IDS) and the Long-Slit Spectrograph (LSS) at both the 1983 (IDS) and 1994 (LSS) apparitions, optical spectrophometry at Mt. Lemmon during the 1994 apparition, and narrowband photometry in 1983 and 1994 from the program centered at Lowell Observatory. Not all of the data have been previously published. We include here newly available results from the 1994 Mt. Lemmon program (an example is shown in Figure 1), for which most of the earlier results were published by Fink and Hicks (1996). We also include newly available results from the observations during the 1994 apparition from McDonald Observatory courtesy of A. Cochran (private communication) and a new reduction of the narrowband photometry from 1983 (Osip *et al.*, 1992; Farnham *et al.*, 2000; Farnham and Schleicher, 2005), for which

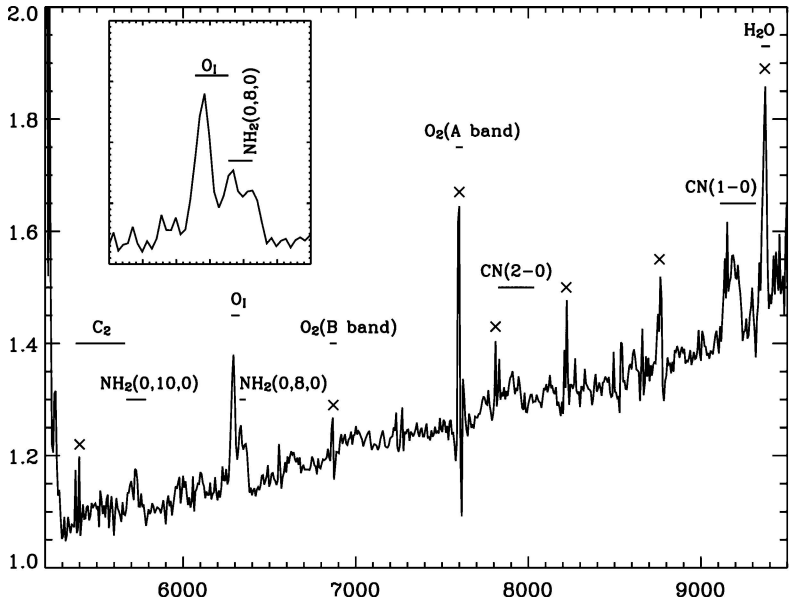

Figure 1. Archival optical spectrophotomteric observation of 9P/Tempel 1. Optical spectrum of Tempel 1 on 12 April 1994, 89 days before perihelion (Fink *et al.* unpublished). The integration time was 6960 s and the vertical axis is in relative units. The prominent cometary emission lines used for analysis have been labeled. Removal of the continuum leads to increased noise and incomplete cancellation of telluric absorption, particularly in the O2 A and B bands. The locations of these spectral artifacts are marked by an 'X'. Note that the zero level for the abscissa has been set much lower than the origin on the vertical scale, in order to emphasize the gaseous coma line emissions. Compared to other comets, Tempel 1 demonstrated relatively strong dust continuum emission relative to weak coma gas line emission.

improved techniques for separating continuum from emission and improved models of atmospheric attenuation in the ultraviolet have now been used, and we include previously unpublished narrowband photometry from 1994. The individual datasets are internally consistent, and variations with time within a given dataset and comparisons with other comets observed by the same groups are appropriate and provide insight into the comet's behavior. Due to the fact that the various groups used different parameters for analyzing the data, the results from different datasets should not be directly compared with each other. We have adjusted the results of Cochran *et al.* (1992) to change from their physically based assumption of expansion velocity to the simpler assumption of $1\,\mathrm{km\,s^{-1}}$ that was used by the other investigators. This removes the largest source of discrepancies between the datasets, but other smaller discrepancies remain. A complete reanalysis of all the data using consistent parameters is beyond the scope of this paper, and we expect that future publications will describe the datasets in much more detail.

COMPOSITION

Reanalysis of the photometric data from the 1983 apparition (Osip *et al*., 1992) and inclusion of the more recent (unpublished) photometric data from the 1994 apparition indicates that, relative to CN, the abundances of the carbon-chain radicals C_2 and C_3 are near the lower edge of the band that defines "typical" cometary chemistry (A'Hearn *et al*., 1995). Cochran *et al.* (1992) found that the carbon-chain radicals, C_2 and C_3, as well as CH have abundances relative to CN that are very near the mean value for all comets in their survey, though we note that their survey included several comets that A'Hearn *et al.* found to be in the "depleted" class. The photometric data also show that, at least in 1994, the abundances of all radicals were low relative to H_2O.

Two unpublished spectra obtained by Fink (as a continuation of the survey program described by Fink and Hicks, 1996) show the abundance of C_2 relative to CN to be low (Figure 1). Using the analysis methods Fink *et al.* applied to their spectroscopic dataset, the average ratios of C_2 and CN with respect to water (parts per thousand) are respectively 0.66 and 1.60. These numbers put comet Tempel 1 in the middle of an intermediate group which they term the "Borrelly type," with CN ratios like P/Halley but with low C_2 ratios like P/Giacobini-Zinner, the prototypical "depleted" comet.

On the other hand, Fink's unpublished 1994 spectra yield NH_2 abundances relative to CN that put Tempel 1 roughly in the middle of the group of 39 comets studied by Fink and Hicks. While this conclusion does not seem to agree with the data in Table VII of Fink and Hicks (1996), newer g-factors require the abundances of NH_2 in that table to be doubled. Cochran *et al.* find in their single measurement of NH_2 during the 1983 apparition that the abundance is very low relative to CN. A'Hearn *et al.* found that the closely related species NH is normal to relatively rich with respect to CN, consistent with the result from Fink's spectra.

Another key aspect of the gaseous abundances is the dust-to-gas ratio. The dust release is measured through optical measurements of the parameter Albedo $\times$ Fill factor $\times$ Aperture radius ($Af\rho$; A'Hearn *et al.*, 1984), which is sensitive to the number density, scattering properties and the size distribution of the dust. At optical wavelengths it provides an estimate only of the amount of small dust particles, with diameters within an order of magnitude of the wavelength of observation. It is thus not a good measure of the total mass of dust in the coma, since the total mass is dominated by the largest particles for plausible size distributions, but it is a good measure of the small dust. Within these limitations, the dust-to-gas ratio in Tempel 1 appears to be moderate. The ratio of $Af\rho$ to the production of OH is 2.3×10^{-26} cm s molecule^{-1}. For comparison, in dust-poor comets like 2P/Encke and 6P/d'Arrest the ratio is $<10^{-26}$ cm s molecule^{-1}, and in dust-rich comets (mostly comets with perihelia beyond 2 AU) it is $>10^{-25}$ cm s molecule^{-1}. Examination of the lightcurves in Figure 2 shows also that, at least over the period for

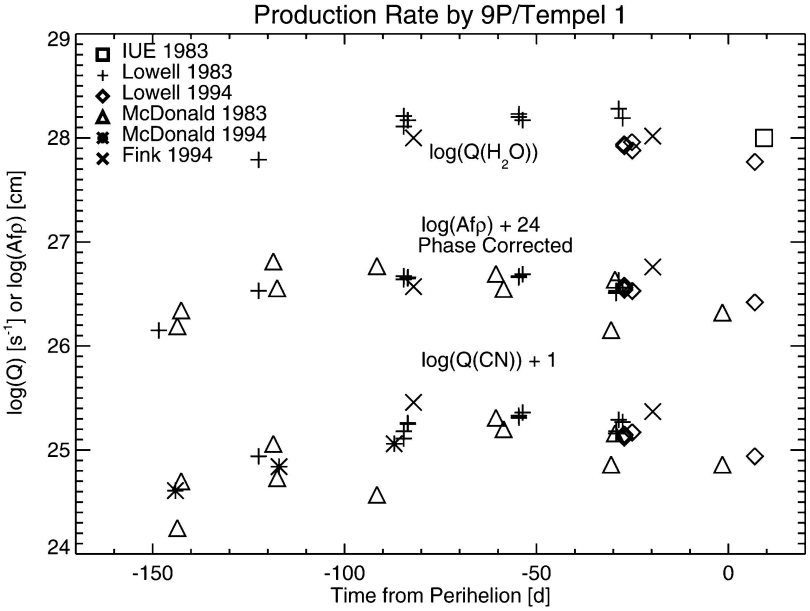

Figure 2. Production rates for OH, CN and dust, from Lowell Observatory narrowband photometry, IUE measurements and IDS spectra from McDonald Observatory. The middle set of data points shows the phase-corrected values of $Af\rho$ from the narrowband photometry as a reference. The lower points show the variation of production of CN from both narrowband photometry and spectrophotometry. The CN and the dust curves both show excellent agreement between the 1983 and 1994 apparitions. The upper points show the production rates of H_2O deduced from narrowband photometry of OH at both apparitions, from IUE spectra of OH (reduced with the same parameters) in 1983 and from ground-based spectrophotometry of $O(_1D)$ in 1994. Unlike the other species (including those not shown here), there may be a factor of two reduction in water production from 1983 to 1994.

which measurements of the gas are available, the gas-to-dust ratio is approximately constant in any apparition.

A comparison with the other comets visited by spacecraft – Wild 2, Borrelly, and Halley – as well as with typical cometary parameters, is given in Table I. Values are nominally for the conditions at perihelion and are based on the work of A'Hearn *et al.* (1995; i.e. not using the reanalysis by Schleicher which does not yet include the other comets), except for the two entries for NH_2, which are from Cochran *et al.* (1992) and from Fink's unpublished spectra. The column headed "typical" is the average of all typical comets in all cases except that of the NH_2 value from Cochran *et al.*, for which it is the average of all comets.

The only other species for which we can compare across a database of many comets is CS, which has been observed routinely in spectra of comets taken with the International Ultraviolet Explorer (IUE) and subsequently with the Hubble Space Telescope (HST). Feldman and Festou (1991) reported on a spectrum taken at the 1983 apparition, and the abundance of CS relative to water is very similar to that

TABLE I
Water production rates and abundance ratios.

	Tempel 1	Wild 2	Borrelly	"Typical"	Halley
$Q(H_2O)$ mol s^{-1}	$\sim 1 \times 10^{28}$	1.3×10^{28}	2.1×10^{28}		1.3×10^{30}
Taxonomy	Typical	Depleted	Depleted	Typical	Typical
Q_{CN}/Q_{OH}	.0015	.0032	.0023	.0032	.0040
Q_{C2}/Q_{CN}	0.81	0.62	0.44	1.1	1.3
$Af\rho/Q_{OH}$	2.3×10^{-26}	4.8×10^{-26}	3.5×10^{-26}	1.5×10^{-26}	4.9×10^{-26}
Q_{NH}/Q_{CN}	1.9	1.5	1.6	1.3	1.6
Q_{NH2}/Q_{CN} C	0.41			0.83	
Q_{NH2}/Q_{CN} F	0.62			0.55	0.85

in comets Kopff and Tempel 2, also presented in that paper, as well as to the values observed in most other comets.

In summary, what we currently know about the chemical composition of the Tempel 1 coma is the following: carbon-chain molecules are at the low end of the "typical" class relative to CN, most radicals are below average relative to water in 1983, and NH_2 (and thus NH) is likely high relative to CN. The dust-to-gas ratio is also well within the range of the "typical" comets, at least as dust can be measured at optical wavelengths. Tempel 1 is thus not clearly anomalous in any way and it is reasonable to assume that, to first order, the composition of its coma in other species not yet observed is also close to A'Hearn *et al.*'s "typical" comet. Though we are not able to measure all of these species with the instruments on Deep Impact, the spatial distributions of the species that we are able to measure should be invaluable in unraveling the appropriate parameters for analyzing Earth-based observations.

VARIABILITY

Figure 2 shows the variation of certain gaseous production rates from comet Tempel 1. We have included the parameter $Af\rho$, plotted with a large offset from zero, as a point of comparison for the shape of the curves of gases. The data for the dust show good agreement among investigators and good agreement from one apparition to another.

The data on gas from Fink have been adjusted to the scale lengths used by A'Hearn *et al.* (see Fink and Combi, 2004, a factor 0.6) and the data from McDonald have been corrected to the assumed expansion velocity of A'Hearn *et al.* (variable but generally between 2 and 3x). In general, the different sources agree well with each other and the shape of the curve repeats from one apparition to the next. For CN, it appears that the scatter is much larger in the data from McDonald than in the data from Lowell, and it is difficult to say whether this is indicative of either temporal or spatial variability, to which the small apertures of the IDS are more sensitive than

the large apertures of the narrowband photometry, or due to some other factor. We note that the dust measurements of Storrs *et al.* (1992; from the same spectra as the results for gas by Cochran *et al.*), for which there are no significant dependences on uncertain parameters, also show a large scatter compared to the results from narrowband photometry (see dust coma section, below). It is clear that the 1983 and 1994 apparitions agree well with each other for the CN, suggesting again that there is little secular change in the comet's activity.

The behavior of water, however, may be quite different. We have converted the narrowband photometric observations of OH to production rates of H_2O (assuming the usual vectorial model) and plotted them in Figure 2, together with the value deduced from the IUE observation in 1983 (Feldman and Festou, 1991) and the two results from Fink (based on $O(^1D)$ and adjusted for differences in scale length). These data suggest a possible factor of 2 decrease in the production rate of H_2O from 1983 to 1994 and thus a corresponding increase in the ratio of all species to water between the 1983 and 1994 apparitions. If this effect is real (the limitations in both ground-based and IUE datasets prevent us from asserting confidently that the variation is real), there are no data that would allow us to distinguish between a secular decrease and random fluctuations from one apparition to the next.

Another observation of Tempel 1 with IUE, not shown in Figure 2, was obtained on July 14, 1994, 11 days post-perihelion, less than 2 days later relative to perihelion than the observation in 1983 (Haken, A'Hearn, and Feldman, unpublished). At that time, approaching the end of IUE's lifetime, there was a large amount of scattered light in all IUE observations taken at moderate solar elongation and this had significant deleterious effects on the tracking, which at that point was already being done in a 2-gyro mode. The resultant fluxes, therefore, are rather uncertain. A best effort to analyze these data yielded a water production rate roughly a factor of 2 lower than that deduced from the observation in 1983, for which both the complete set of geometrical circumstances and even the solar activity were nearly the same. Although there are always large uncertainties in correcting ground-based observations of OH for atmospheric extinction, and although the second IUE measurement was uncertain for instrumental reasons, we have some confidence that the factor of 2 change in water release between the two apparitions is real. The change shows up independently in comparing ground-based observations in June 1983 to those in June 1994, in comparing space-based observations in July 1983 with those in 1994, and in comparing the ground-based measurements in July 1994 with the space-based measurements in July 1983. All three comparisons show the water production to be higher in 1983 than the 1994, making it unlikely that the difference is due to calibration uncertainties or instrumental problems. On the other hand, all indications are that the nucleus is in a state of simple rotation (the repeatability of seasonal variations, similarity in features at a given point in the orbit, etc.), so the progression of solar illumination on the nucleus follows the same pattern on each perihelion passage, reducing the possibility that different sources are illuminated on different apparitions. We can present no compelling scenario to explain why

the water production drops by a factor of 2 from one apparition to the next while production of other species remains essentially constant. Clearly, an understanding of the spatial distribution of the water in the inner coma relative to the distribution of other species will be an important goal of Deep Impact's encounter.

The Dust Coma

Useful observations of dust in cometary comae have been obtained from UV through sub-mm wavelengths and include spatial imaging, photometry and spectroscopic measurements. For low-activity comets like Tempel 1, where flux limitations are a concern, only broadband optical photometric observations are commonly obtained. Fortunately for studies of the dust, the observed flux in these broadband filters is dominated by the continuum, and these observations work well to characterize the long-term behavior of the comet's activity. To obtain information about the dust composition and particle size distribution (PSD), which are critical for quantifying the mission risk during the Deep Impact encounter, longer wavelengths – IR and beyond – are used. Specifically, the 10–1000 μm wavelength regime is most sensitive to the grains larger than 100 μm that pose the largest impact and navigation hazards to the spacecraft.

The dust coma data fall into three broad categories – temporal (lightcurves), morphological, and spectrophotometric. We discuss each in turn below.

Temporal Behavior (Lightcurves)

The long-term gross behavior of the Tempel 1 coma can be elucidated from photometric measurements obtained around the comet's orbit (Figure 3). We use the parameter $Af\rho$ (A'Hearn *et al.*, 1984) for interpreting the long-term optical photometry, because it removes the variations introduced by changing geocentric and heliocentric distance, aperture size differences, etc. In this work we also refer to the parameter $\varepsilon f\rho$ as an analogous quantity for interpreting infrared observations of the dust. For $\varepsilon f\rho$, where the measured flux is assumed to be the thermal emission from a blackbody at the local equilibrium temperature instead of the incident light scattered at the observed phase angle.

A number of observations of Tempel 1 exist as unpublished observations and as individual astronomical circulars. The sum of these scattered observations has led to phenomenological claims of variable dust and gas production rates pre- and post-perihelion. To further investigate this issue, we adopted instead the assumption that the comet's temporal behavior is the same from one apparition to another and assembled a long-term lightcurve covering a two-year period around perihelion for the best observed species, dust. For this lightcurve, we combined several data sets to provide good temporal coverage of the perihelion portion of the comet's orbit. These data include the 1983 InfraRed Astronomy Satellite (IRAS) measurements (re-analyzed as discussed below), the 1983 optical photometry of Cochran *et al.*

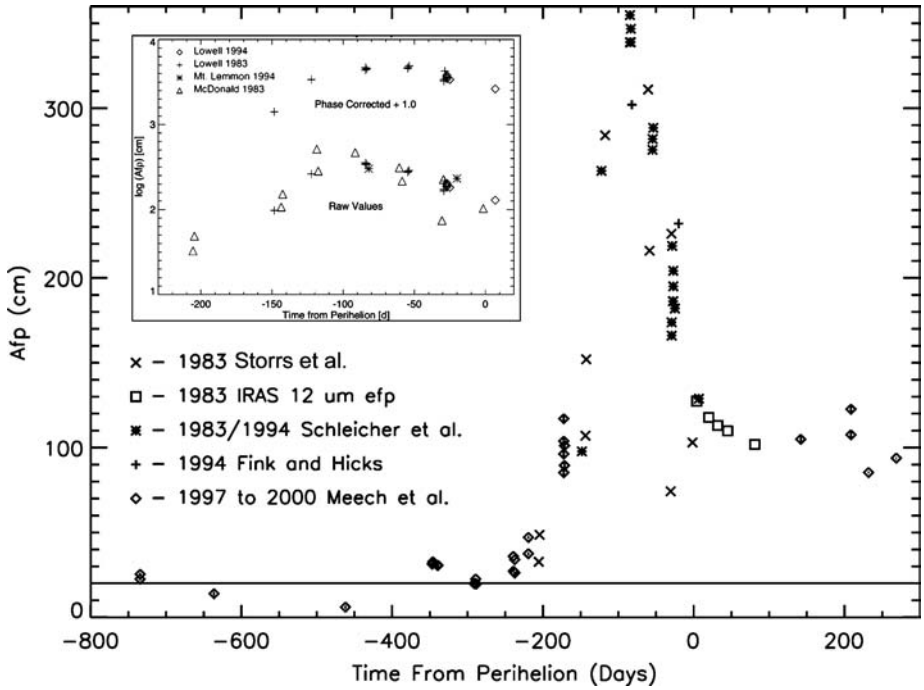

Figure 3. As-observed long term lightcurves for 9P/Tempel 1 derived by overlaying the $Af\rho$ and $\varepsilon f\rho$ measures from the 1983, 1994, and 1999 apparitions, plotted with respect to time of perihelion. The optical $Af\rho$ measurements of Osip *et al.* (triangles) and Meech *et al.* (diamonds) have estimated errors of 15%. The IRAS $\varepsilon f\rho$ points (squares) have estimated errors of 25%, including systematics. The temporal behavior is generally consistent between the three apparitions, suggesting the comet's behavior is repeatable from orbit to orbit and that the $\varepsilon f\rho$ behavior reflects the trends seen in $Af\rho$. The emission rate of dust is quite different before and after perihelion, suggesting seasonal illumination of the actively emitting surface regions. The solid line denotes the $Af\rho$ value expected for a bare nucleus with no dust emission. Inset – $Af\rho$ values corrected for the phase-angle variation of scattering. The narrowband photometry was obtained at λ 4845 Åfor most of the observations, though a few were obtained at λ 5240 Å. McDonald Observatory measurements (Storrs *et al.*, 1992) were obtained at λ 4800 Å while those from Mt. Lemmon are at λ 6250 Å. The narrowband photometry shows the best internal consistency, possibly because it averages out spatial and temporal variations on small scales to which the spectroscopic techniques are sensitive. The top curve shows the $Af\rho$ values that are derived from the narrowband photometry when corrected for the solar phase angle (using the scattering function of Ney and Merrill (1976)). The correction makes the curve much broader with the peak production near −60 days rather than near −85 days, bringing it into agreement with the maxima in the H_2O and CN gas production rates (Figure 1).

taken from the McDonald Observatory, the extensive 1999–2000 optical photometry from Meech *et al.* (2005), and the narrowband optical photometry of Schleicher *et al.* for the 1983 and 1994 apparitions. (We note that the scatter in the data from the IDS at McDonald Observatory is much larger than the scatter in the data from the narrowband photometry. It is not clear why this is the case, but we suggest that it is due at least in part to the relatively small effective aperture in IDS, and to the

fact that some of the observations were offset from the nucleus, which makes those measurements much more sensitive to both temporal and spatial variability in the outgassing).

The resulting composite lightcurve indicates that the observations of dust in 1994 and 1997–2000 are, for the most part, consistent with the observations from 1983, suggesting there is little secular variation in the comet. The lightcurve rises rapidly, starting about 8 months before perihelion, apparently peaking around −90 days, and falls off more slowly through and after perihelion. There is still evidence of coma nearly a year after perihelion, at which time the comet is beyond 3 AU from the sun. This continued level of activity is likely due to very slow dissipation of slow-moving dust as the gas production decreases near the ice line, with a concomitant decrease of the terminal velocity of the dust and increase in the dust lifetime in the coma. Another possible cause of the post-perihelion persistence of emission is the time lag for the turnoff of volatile emission created by the propagation of the thermal wave driven by the comet's perihelion passage. The comet interior will be on the whole warmer 6 months after perihelion passage than 6 months before. Without high precision imaging of the gas coma with the comet at the ice line, or detailed nucleus thermal measurements, we cannot easily distinguish between these two possibilities.

The derived lightcurve also explains the phenomenological reports of a variable pre-/post-perihelion asymmetry. By assuming a peak in activity around perihelion, which our lightcurve clearly shows is not the case, discordant values of the activity are found. As can be seen from Figure 3, sampling the Tempel 1 lightcurve at times spaced equally before and after perihelion would lead to an estimate of the ratio of post-/pre-perihelion activity ranging from a value of 0.5 up to 4.0.

The apparent peak in production 90 days before perihelion is misleading because these data have not been corrected for phase angle variations. In order to account for this, we have taken the dataset from Lowell Observatory, since it shows so much less scatter than the data from McDonald, and applied a phase correction following the work of Ney and Merrill (1976). The result is plotted in the inset of Figure 3, displaced upward by 1.0 in $\log(Af\rho)$. The Ney and Merrill phase function produces the largest change to the figure of the several phase functions we have tabulated in planning the Deep Impact mission, and the true phase correction is probably not this large. However, it is clear that the curve is now much flatter than without correction, and if one tries to pick the peak, it is probably near 60 days pre-perihelion rather than the earlier time deduced from the uncorrected lightcurve. In either case, the early peak indicates that there is some kind of seasonal variation affecting the production rates.

Even with this offset in the peak activity, however, there seems to be little influence from non-gravitational forces on the orbit, since the force parameters are relatively small (Marsden and Williams, 2003; Yeomans *et al.*, 2005). This implies that either the gas and dust emission are not consistently directed in a preferred direction, or else the force from the directed emission is very small relative to the mass of the nucleus.

DUST MORPHOLOGY

The dust coma is created when hydrodynamic drag by the outflowing gas lifts dust grains off the surface of the nucleus. At a distance of 10–100 nuclear radii, the gas and dust decouple, leaving the dust particles in their own independent orbits around the sun, where the opposing forces of solar gravitation and radiation pressure govern the particle motions (Combi *et al.*, 2005). In the most basic scenario, a nucleus undergoing constant, isotropic dust emission will produce a coma that starts out spherical, but elongates with time as the grains are swept back into the tail by radiation pressure. The efficiency of radiation pressure on the grains is related to the ratio of cross-sectional area to mass, so small grains are accelerated down the tail much more rapidly than large grains, effectively acting to "sort" the different particle sizes (Finson and Probstein, 1968). Because the basic forces on the dust are purely radial with respect to the Sun, the coma and tail spread out along the comet's orbital plane, though there will be some finite thickness above and below the plane due to the dust's out-of-plane velocity at the time of the gas/dust decoupling.

Many comets, on the other hand, are not dominated by isotropic emission but also have isolated active regions that produce very narrow jets (cf. comets Borrelly and Wild 2). These jets are superposed over the symmetric emission morphology and appear as structure or features in the coma. (We also point out that the isotropic emission in a comet may actually be produced by lateral diffusion of jet material, by the contributions of a large number of distributed weak jets, or by some other mechanism, but the result can be indistinguishable from isotropic emission when observed at large distances.) Depending on the strength of the jet or jets, it may be necessary to process images of the coma to clearly reveal these features, but strong jets can be clearly visible in raw images. Here we apply systematic techniques described by Schleicher and Farnham (2005) to search for features produced by directed emission from the nucleus.

Previous studies of Tempel 1 in the literature (Campins *et al.*, 1990; Lynch *et al.*, 1995; Fernandez *et al.*, 2003) reported what appears to be a featureless, smooth coma, suggesting the emission is isotropic or comes from multiple sources that mimic isotropic outflow. However, even if jets are present, they may not be resolved on the alternate unfavorable apparitions. For example, the most recent apparition, in 2000, was a poor one, and even with the wealth of CCD data that was obtained by the Deep Impact project for the newly designated mission target, no features have yet been detected (Figure 4a). On the other hand, out of only a few CCD images that are available from the 1994 favorable apparition, a broad fan jet is clearly distinguishable (Figure 4b). This feature is visible in all the available images, from mid-March, mid-April, and mid-June (-108, -82 and -21 days from perihelion). It is clear from both the March and June images that the fan cannot be modeled exclusively using radiation pressure forces. Thus it is not a dust tail but instead must be produced, at least in part, by directed emission from an active

source on the nucleus. The surface brightness in the jet is about a factor of 2 higher than the average coma surface brightness (at any given distance), so, given the margin of error in the hazard analysis (see the discussion below), the increased dust density within the jet is not a significant concern for the DI spacecraft. No calibration

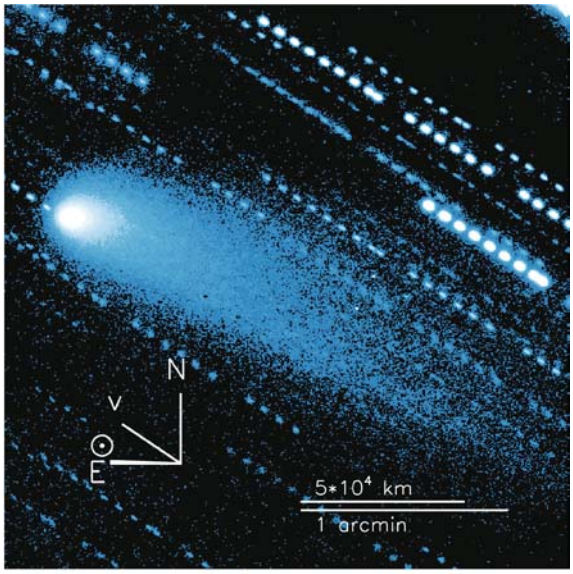

(a)

Figure 4. Archival coma images of Tempel 1. a) UH 88″ R-band image of Tempel 1 on 21 August 2000, at 202 days after perihelion, $r = 2.54$ AU, $\Delta = 1.67$ AU. North is up and East is to the left. The coma is relatively active in this image, but appears featureless, though a weak tail is apparent. b) Clear filter (3500–10000 Å) image of Tempel 1 on 17 March 1994 (from Fink *et al.*), enhanced by removing a ρ^{-1} profile to show the fan jet. North is at the top, East is to the left and the field of view is 78000 km × 78000 km. The jet is visible pointing to the southwest. The most likely cause is directed emission from the nucleus. Syndynes (dashed) and synchrones (solid) have been overlaid to show the motion of dust under the influence of solar radiation pressure. The fact that the fan is not aligned along the syndyne/synchrone direction indicates that the feature is not produced by the interactions of solar gravity and radiation pressure (e.g., it is not the dust tail). Although the jet appears to lie in the anti-solar direction, this is likely a projection effect. The solar phase angle on this date was only 14.9°, so nearly the entire Earth-facing side of the nucleus is illuminated. c) IRAS survey imaging of 9P/Tempel 1 on 28 July 1983, $r = 1.56$ AU, $\Delta = 1.27$ AU. This 12-μm reconstructed survey image with 24″ per pixel resolution has the highest SNR and largest extent of the four IRAS passbands. South is to the top and West is also to the left. The comet is moving towards the lower right, and the projected direction to the Sun is to the lower right. There is little structure evidenced by the coma, other than some extension in the anti-solar direction, as expected from dynamical modeling of a low-inclination comet. This image, taken near perigee in 1983, also shows a hint of the comet's linear trail structure, composed of large, heavy dust particles. Inset – large scale 12 μm image of the comet, 1.5° × 1.5°, clearly showing the large extent of the comet's trail. The comet nucleus is the bright point in the center, and the comet trail extends mainly north and west in the anti-velocity direction, i.e. along the orbital path the comet has recently traveled.
(*Continued on next page*)

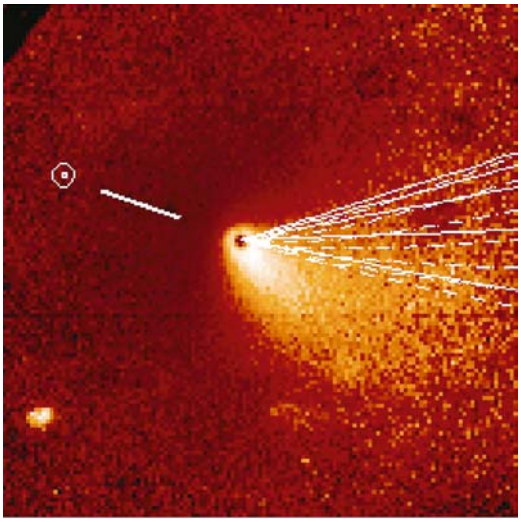

(b)

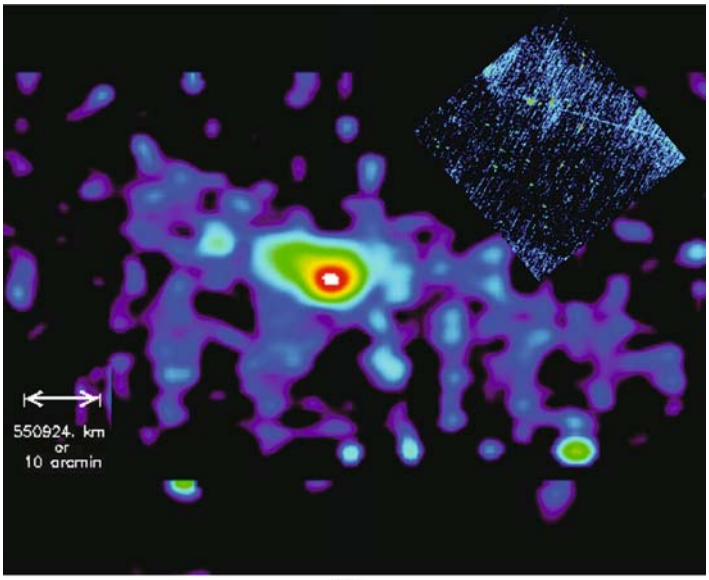

(c)

Figure 4. (*Continued*)

information is available for these images, so it is not known exactly how the absolute surface brightness changes from month to month, but the jet is much more well-defined in March and April, when the coma activity was increasing towards its peak, than in June, when the activity was dropping. In addition to the CCD images, at least two experienced visual observers have detected features in the coma. Both of these detections, in April 1983 (J.C. Merlin, private communication) and May 1994

(N. Biver, private communication; see Belton *et al.*, 2005, Figure 8), were obtained when the comet was relatively close to Earth, providing good opportunities for resolving features.

These three sets of observations are currently the only ones known to show coma morphology. The existence of the jet also indicates that the nucleus has isolated active areas, which is consistent with the result from the models of Groussin *et al.* (2004) that conclude only about 8% of the surface area is active. Interestingly, the features have been observed in the coma only at times when the production rates were near their pre-perihelion peak (Figure 3) and this suggests that the jet and the time of peak emission may be related (e.g., at the time of peak activity, the sun is at its highest point in the sky as seen from the source that produces the jet). We qualify this conclusion with the caveat that the dearth of high-quality optical imaging data in the post-perihelion time frame may introduce significant selection effects.

The shape and appearance of a jet in the coma is dependent on a number of factors: the size and location of the source, the rotation state of the nucleus, the motion of the comet in its orbit, and changes in the viewing geometry of the comet. With sufficient observations, it is possible to use coma models to extract many of these properties, helping to constrain the nature of the nucleus. Unfortunately, the number of currently available images of Tempel 1 that show features is too small to constrain the models. The 2005 apparition, however, will be a favorable one, and the conditions will be such that high-resolution images of the coma can be obtained for several months before perihelion. With the observing campaign in support of the Deep Impact mission, a massive amount of data will be obtained before and after perihelion (=impact), and these data will help to characterize the features that are seen.

Finally, there is another morphological feature that should be mentioned. In July and August 1983, IRAS observed Tempel 1 at 12, 25, 60, and 100 μm. A sample 12-μm image, chosen because the 12 μm passband tends to have the highest signal-to-noise, is shown in Figure 4c. In these images, the coma and tail are only slightly more extended than the instrumental point spread function, with little of the extension along the Sun-comet vector that would be expected for small dust particles highly accelerated by solar radiation pressure (Lisse *et al.*, 1998). It may be that the dust production had dropped significantly so that the small grains were barely detectable. However, the IRAS images do show evidence of a faint dust trail consisting of large dust particles, which can be seen more clearly in large-scale ($3^\circ \times 3^\circ$) IRAS Sky Survey images (Sykes, 1992: Inset, Figure 4c). For the biggest grains emitted from the nucleus ($>1000\,\mu$m), the emission velocity is small, and radiation pressure is essentially negligible, so they have orbital paths very close to that of the nucleus. Over time, these large grains spread out along the comet's orbit to form a trail that can be observed when the Earth is near the comet's orbit plane. The existence of this trail indicates that large grains could be a danger for the flyby spacecraft, though the actual size and number density of these particles is difficult to predict precisely – only the total particle surface area can be determind

for the IRAS measurements. To minimize the hazard from these particles, the DI encounter was designed to pass through the comet's orbital plane (where the large grains are concentrated) after the point of closest approach, and thus after the main sequence of observations have been obtained.

DUST SPECTROPHOTOMETRY

Spectrophotometry of comet 9P/Tempel 1 was obtained by IRAS in four broad bandpasses at 12, 25, 60, and 100 μm and by the IRAS 8–21 μm Low Resolution Spectrometer (LRS) in July–August 1983. These observations, along with 5240 Å narrowband continuum photometry taken contemporaneously (Osip *et al.*, 1992), can be combined to produce a 0.5–100 μm spectral energy distribution (SED; Figure 5), after correcting for the different aperture sizes of the instruments assuming a ρ^{-1} coma brightness profile.

While relatively sparsely sampled in wavelength compared to other comets we have studied, the combination of thermal infrared and optical observations is quite sensitive to the 0.1–100 μm range of dust particle sizes emitted by comets (Lisse *et al.*, 1998). The lack of a strong 8–13 μm silicate emission feature is an indicator of the abundance of relatively large dust grains ($\geq$10 μm), as is a spectral color temperature of $\sim$245 K, within 10% of the local equilibrium temperature, and close agreement to greybody behavior at 30–100 μm (Harker *et al.*, 1999; Mason *et al.*, 1998). The total albedo for scattering, defined as the ratio of the scattered luminosity to the total integrated luminosity over all wavelengths, is $8 \pm 2\%$ (2σ) for Tempel 1, similar to the $\sim$6% found for the large cometary dust particles emitted by comets C/Austin 1990 V (Lisse *et al.*, 1994, 1998) and 2P/Encke in 1997 (Lisse *et al.*, 2004).

Modeling of the scattering and thermal emission spectrum (Lisse *et al.*, 1998, 2004), using the energy balance between absorbed visible photons from the 5750 K solar radiation field and the thermal infrared radiation emitted by the dust was used to further constrain the silicate: refractory carbonaceous material composition ratio and particle size distribution of the dust. Following the results of the Halley encounters (Jessberger *et al.*, 1988; Jessberger and Kissel, 1991), the particles contributing appreciably to the SED are assumed to be spherical with a radius of $0.1\ \mu\text{m} < \mathbf{a} < 10^4\ \mu\text{m}$. We also assume a porosity and density $\rho(\mathbf{a})$ for the dust as a function of particle size, so that the mass of a particle as a function of particle radius is given by $m(\mathbf{a}) = 4/3 \times \rho(\mathbf{a})\mathbf{a}^3$. The dust composition is modeled as a material with index of refraction given by a Bruggeman mixture (Lien, 1990) of the indices for silicates, water ice, amorphous carbonaceous material, and vacuum with density $\rho = \rho_o(a/0.1\ \mu m)^{(D-3)/D}$ (where D is the fractal dimension of the dust and $\rho_o = 2.5\ \text{g cm}^{-3}$). The velocity of emission is derived from dynamical modeling of the coma and tail morphologies of other short-period comets (Finson and Probstein, 1968; Sykes *et al.*, 1990; Lisse *et al.*, 1998) and is on the order of $0.3\ \text{km s}^{-1}$ X $\sqrt{}(10^{-4}/\text{a (cm)})$. Following Fernandez *et al.* (2003) and Lisse *et al.* (2005),

the nucleus was assumed to have thermal emission following a standard thermal model (Lebofsky and Spencer, 1989), $r_{\rm eff} \leq 5$ km, emissivity = 0.90, beaming parameter = 0.90, geometric albedo = 0.05 ± 0.02, a visual phase coefficient of 0.065 magnitudes, and an infrared phase coefficient of 0.01 magnitudes deg^{-1}. In all

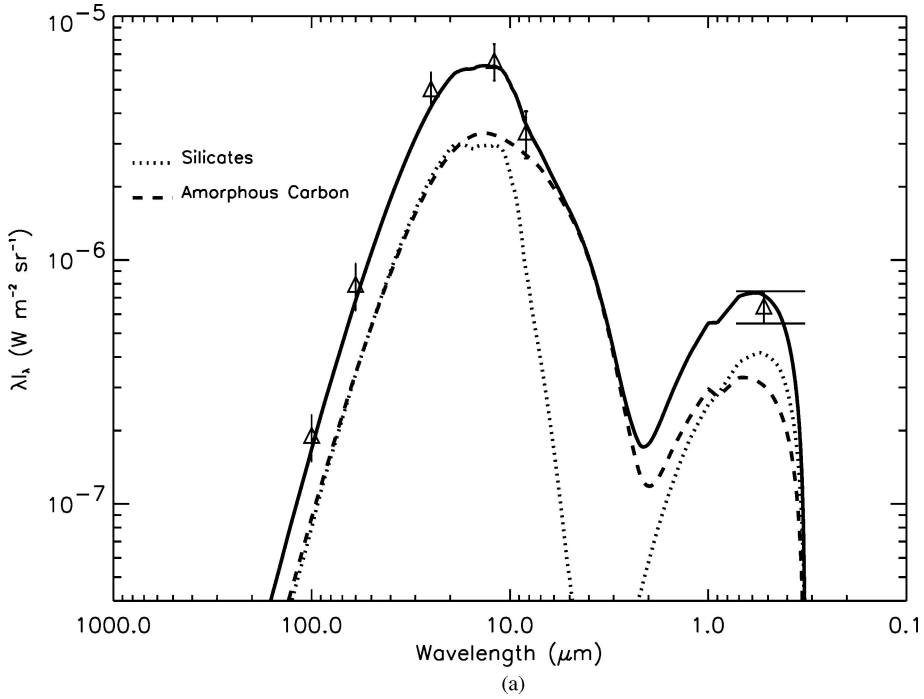

(a)

Figure 5. Dust coma spectral energy distribution and spectral model fits for 9P/Tempel 1. a) The coma spectral energy distribution is derived from recalibrated broadband IRAS flux measurements taken near perigee on 12 July 1983. All error bars in this and subsequent plots are $\pm 2\sigma$. The recalibrated fluxes are consistent with a greybody out to 100 μm. Solid curve – Best fit modified Mie model to the data, with 50% astronomical silicate, 50% amorphous carbon content, $\rho = \rho_o$ (m/10^{-14} g)$^{-0.10}$ density law, and a m$^{-0.75}$ particle mass distribution. Of the tested plausible size distributions, only power law particle size distributions produce spectral energy distributions that fit the data adequately. Dotted line – flux emission due to silicate grains, which dominates at wavelengths >8 μm and is responsible for the emission features at 8–13 μm and the long wavelength falloff. Dashed line – flux emission due to amorphous carbon grains, which dominates at 3–8 μm and is responsible for the "superthermal emission" at 3–5 μm. The derived $Q_{\rm dust}$ for this model is 220 kg s^{-1} with an albedo of 9%. The 95% confidence level ranges for these parameters are 190–400 kg s^{-1}, and 7–10% albedo. b) χ^2 surface for allowed models with density = p_o (m/10^{-14} g)$^{-0.05}$. The abscissa coordinate is the percentage of silicaceous material in the silicate:refractory carbonaceous material composition used to model the spectral energy distribution (SED). The ordinate is the power law index in the particle mass distribution $dn/d\log m \sim m^{-\alpha}$ used to model the SED. c) χ^2 surface for allowed models with density = p_o (m/10^{-14} g)$^{-0.10}$. While the allowed power law index is limited to the range $0.64 < \alpha < 0.75$, and the dust density index to the range $0.05 < \eta < 0.10$, the material composition of the dust is poorly constrained by the data.

(*Continued on next page*)

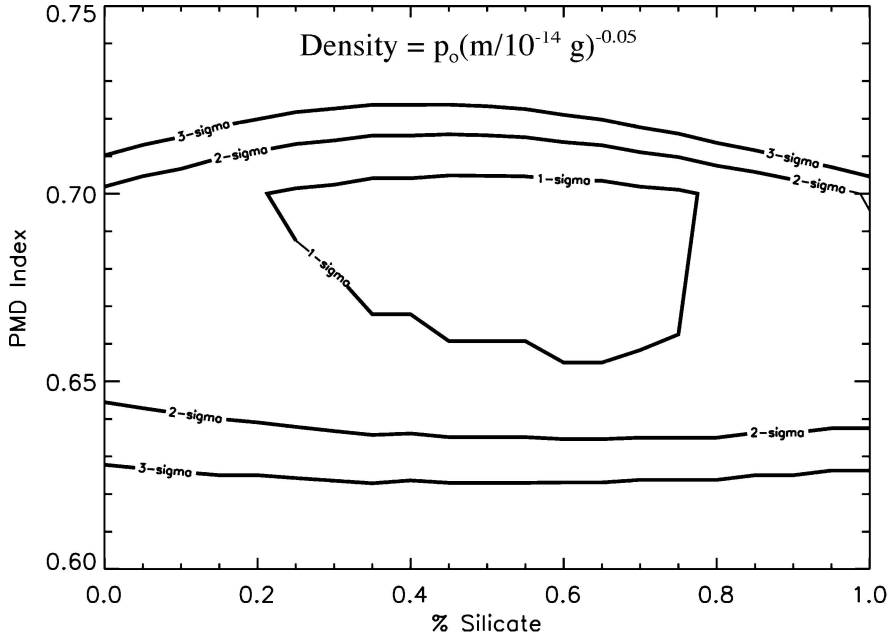

(b)

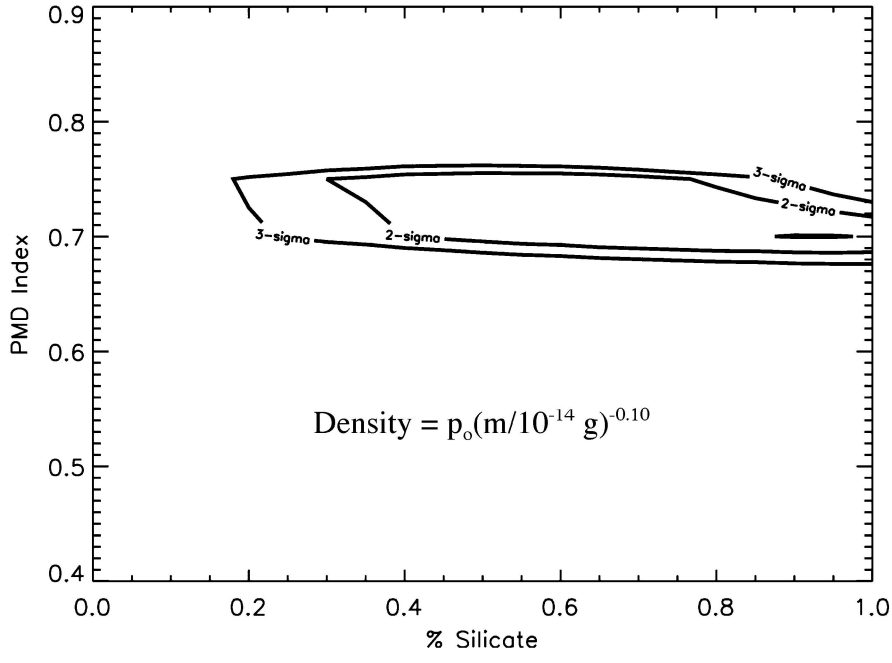

(c)

Figure 5. (*Continued*)

models, it is found that the nucleus flux contribution is trivial compared to the dust flux. This is consistent with the longterm lightcurve shown in Figure 3 – at the time of the IRAS observations (0 to +60 days) the signal from the dust is still a factor of 5–7 times higher than the asymptotic flux found when the comet is at aphelion (depicted by the horizontal solid line) that represents the contribution from the nucleus.

The allowed range of dust models (Figures 5b and 5c) is strongly constrained by the combination of mid-IR and optical photometry – for size distributions with an underabundance of small particles, little scattering occurs and the optical flux is too low; for size distributions with an overabundance of small particles, the predicted optical flux is too high, the dust is too warm, and a strong silicate feature (for non-zero silicate compositions) is predicted. At the 95% confidence level only models with size distribution $dn/d\log m \sim m^{-\alpha}$, $0.65 < \alpha < 0.75$, density $\rho = \rho_o(\mathbf{a}/0.1\,\mu m)^{-0.25\,\mathrm{to}\,-0.40}$ (fractal dimension $D = 2.76 \pm 0.06$), and nucleus of radius r_{eff} between 2 and 3.5 km, were consistent with the observed thermal emission spectrum. (This implies coma dust particles with effective density ranging from $2.5\,\mathrm{g\,cm^{-3}}$ at radius $0.1\,\mu$m to $0.44\,\mathrm{g\,cm^{-3}}$ at radius 1 cm). The silicate:carbonaceous composition ratio was poorly determined by the essentially featureless SED. No water ice was required for the best-fit models, as expected for warm outer coma dust inside the solar system ice line at ~3 AU (Lien, 1990). The allowed particle size distributions (PSDs) are surface-area and mass-dominated by the largest particles ($\mathbf{a} > 100\,\mu$m). The emission rate of dust released by the comet was found to be in the range 100–390 kg $\mathrm{s^{-1}}$ ($\pm 2\sigma$), depending on the model adopted.

Comparison to 11 other comets we have photometrically surveyed for dust properties (Lisse *et al.*, 2002, 2004; Figure 6) shows Tempel 1 to be a typical short-period comet of average dust activity, composition, and size, emitting mainly large (10–1000 μm), dark (average albedo $= 8 \pm 2\%$) particles. The higher albedo found for the coma dust (8%) versus the nucleus surface (5%) suggests a relative enrichment in dark absorbing material on the surface of the nucleus as compared to the composition of the coma dust, an effect which could be caused by surface mantling.

Practical Implications for the Deep Impact Mission

Spacecraft Trajectory and Target Acquisition

The dust optical depth for the coma (and its associated trail) are low from the best-fit greybody models for the observed SED's, less than 3×10^{-7}, so no obscuration of the nucleus by the dust is expected in the Deep Impact flyby images during encounter. We can, however, expect that the pixels detecting emission from the nucleus will also be detecting coma emission. On the spacecraft's

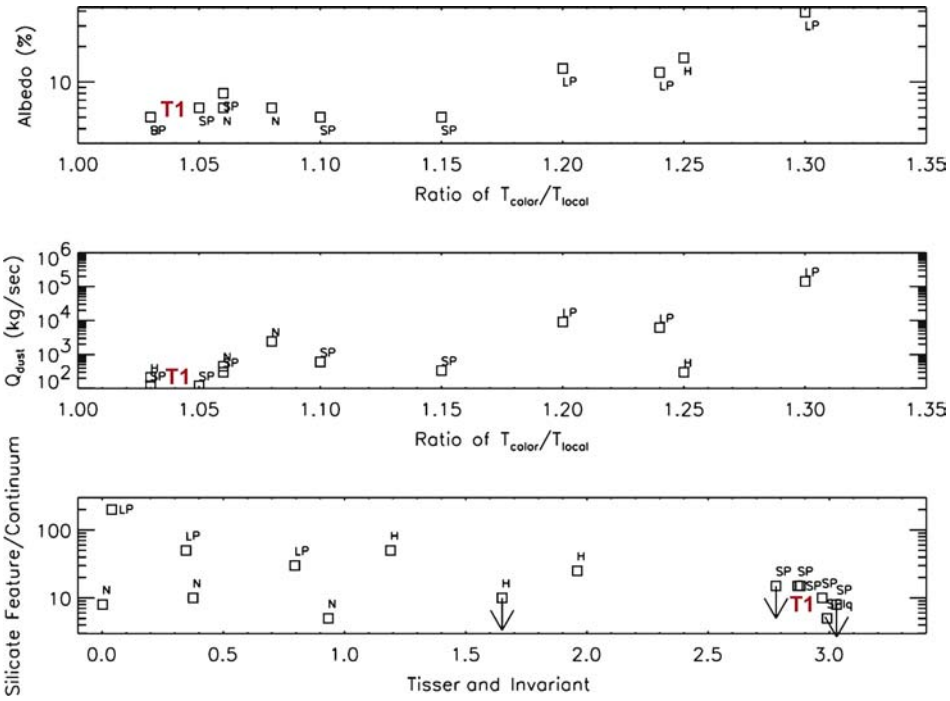

Figure 6. Comparison of Tempel 1 dust properties to those of other comets. Correlations in the observations of emitted cometary dust by albedo, silicate feature amplitude/continuum ratio, dust color temperature, $Q_{\rm dust}$, and Tisserand invariant of the parent comet from the Lisse *et al.* (2002) survey. Long-period comets produce the most dust with the hottest color temperature, highest albedo, and largest silicate feature. The new and short-period comets produce little dust, and what they do produce is cold and low albedo, with little or no silicate feature. The Halley comets lie between the two extremes. Tempel 1 fits in this scheme as a typical short-period comet of average dust activity albedo, and particle size. (T1's location in the dust survey is denoted by the red T1 label.)

approach, the coma emission will dominate over the nuclear emission until the spacecraft is close enough to the comet that the effective dust surface area in a projected pixel area drops below that of the nucleus surface area contained in the pixel.

An estimate of the measured signal per pixel is given in Figure 7. Here we have assumed an 8% dust scattering albedo and a Halley-like phase law for the dust, a 5% geometric albedo for nuclear scattering, a phase-angle dependence for nuclear scattering found for 2P/Encke 1997 (Fernandez *et al.*, 2000), a dust production rate of $230\,{\rm kg\,s^{-1}}$, and DI High-Resolution Imager pixel dimensions of $4\,\mu{\rm rad}^2$. The nucleus signal flattens out when the nucleus becomes resolvable, i.e., when the signal per pixel becomes a nucleus surface brightness issue, and not the distance to a point source. Coincidentally, but independently, the signal for the coma begins to flatten out when we start to traverse inside the coma, at about

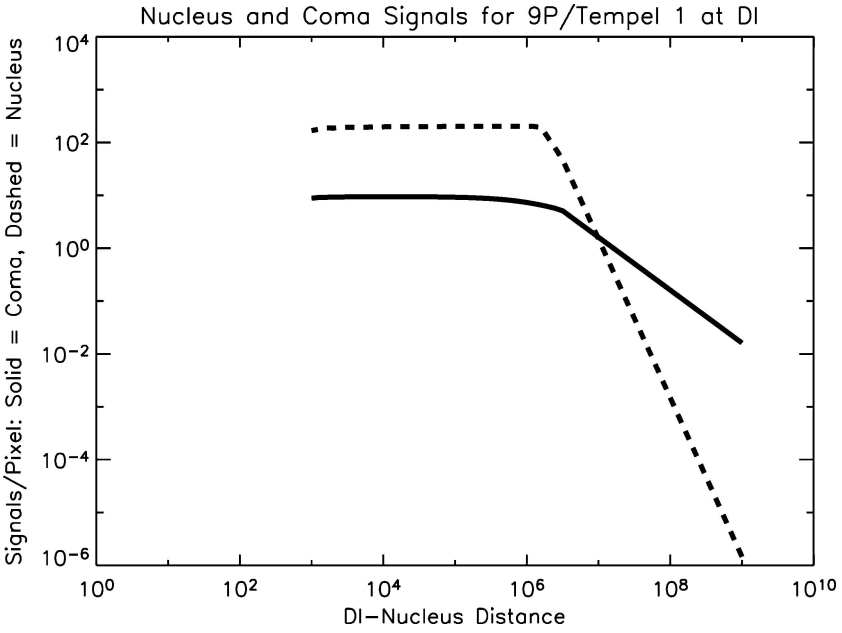

Figure 7. Nucleus/Coma Contrast. Estimated brightest pixel V-band fluxes for 9P/Tempel 1 in the HRI imager during the Deep Impact encounter, as a function of the spacecraft–nucleus distance. The large changes in slope of the two curves occur when the nucleus and coma become resolvable. Each curve has been corrected for the estimated scattering phase function. The horizontal axis has units of km, and the vertical axis has units of number of photons $\mathrm{cm}^{-2}\,\mathrm{s}^{-1}\,\mu\mathrm{m}^{-1}$.

1×10^6 km distance to the nucleus. The nuclear signal becomes comparable to the coma signal at a distance of $\sim 8 \times 10^6$ km or $\sim 8 \times 10^5$ s (9.1 days) before impact.

As a check of this calculation, we scaled our Tempel 1 model to the circumstances for the Deep Space 1 flyby of P/Borrelly on September 22, 2001 [$v_{\mathrm{encounter}} = 16.5\,\mathrm{km\,s}^{-1}$, $Af\rho = 646$ cm at perihelion/encounter, flyby distance $= 2000$ km, DS-1 pixels $\sim$5 times larger than the DI HRI pixels, $r_{\mathrm{nucleus}} = (4\,\mathrm{km} \times 2\,\mathrm{km})$], and found that the nucleus signal should have been comparable to the coma signal at about 1×10^5 s or 1.6×10^6 km before closest approach. The DS-1 mission detected the nucleus of comet 19P/Borrelly at about 3×10^6 km from the nucleus, in good agreement with our model predictions (D. Yeomans, private communication).

The dust coma morphology in the IRAS thermal infrared images appears relatively isotropic, with at most one pronounced jet of moderate strength (Figure 3). There is thus no expected region of minimized coma dust density for the spacecraft to fly through. The trail emission discussed earlier, however, is clearly much brighter "behind" the comet, i.e. along the orbital path in the direction the comet has already traveled, with an expected maximum in the orbital plane of the comet. The trail width from the IRAS images is on the order of 1×10^5–2×10^5 km,

similar to the width of the Encke trail found by Reach *et al.* (2000) using the Infrared Space Observatory (ISO). Thus the Deep Impact flyby spacecraft will be traversing the trail at closest approach. The overall risk to the flyby spacecraft can thus be minimized by choosing an encounter geometry that crosses through the orbital plane as late as possible, in the direction of the orbit that the comet has just traversed, after the impactor hits the surface and crater formation has occurred.

Mission Hazard Minimization and Expected Dust Burden

The two parts of Deep Impact, the impactor and the flyby spacecraft, will each take separate, close trajectories through the coma of comet P/Tempel 1. The spacecraft will encounter dust and gas emitted from the comet's surface at roughly 10 km s^{-1} relative speed of the spacecraft with respect to the nucleus and at distances up to 10^4–10^5 km from the nucleus. In order for the DI mission to succeed in returning useful science data, it is important for the spacecraft design to be able to deal with the effects of the coma environment on the spacecraft. The most critical of these effects arises due to dust impacts on the spacecraft at high relative velocities, which can cause both damage to the spacecraft and its instruments and tumbling of the spacecraft orientation. Here we discuss the expected number of dust grain impacts on the two spacecraft.

The fundamental problem in estimating the amount of dust hitting the DI spacecraft, or dust flux, is determining the spatial number density (number per $meter^3$) of dust of radius **a** (cm) in the coma around the comet's nucleus as a function of distance from the comet. We must integrate along the spacecraft trajectory through this spatial distribution to find the total dust "fluence." The impactor will encounter dust along a trajectory through the coma, modeled as a line of sight (LOS) spacecraft-comet distance that ranges from a value of infinity to 3 km, where the impactor encounters the nuclear surface. The flyby spacecraft will encounter dust along a path through the coma with an impact parameter of 500 km as well as a possible enhancement in the size and number density of the grains, when it crosses the comet's orbital plane and encounters the dust trail.

To estimate the dust impact burden on the Deep Impact spacecraft during the mission, we have constructed a model coma assuming hemispherical sunward driven emission, a dust particle size distribution obtained from the IRAS spectral modeling results, and total amount of dust surface area at perihelion normalized to the $Af\rho$ curve of Figure 3. We find a total estimated dust particle fluence for the DI flyby spacecraft traveling from infinity to an impact parameter of 500 km as shown in Figure 8. The ordinate represents the total predicted number of particles of each mass encountered along a chord through the coma. The results for the impactor spacecraft will be exactly the same, scaled by a factor of (500 km/3 km) minimum distance X 0.5 (since the impactor traverses only one-half the coma). The total

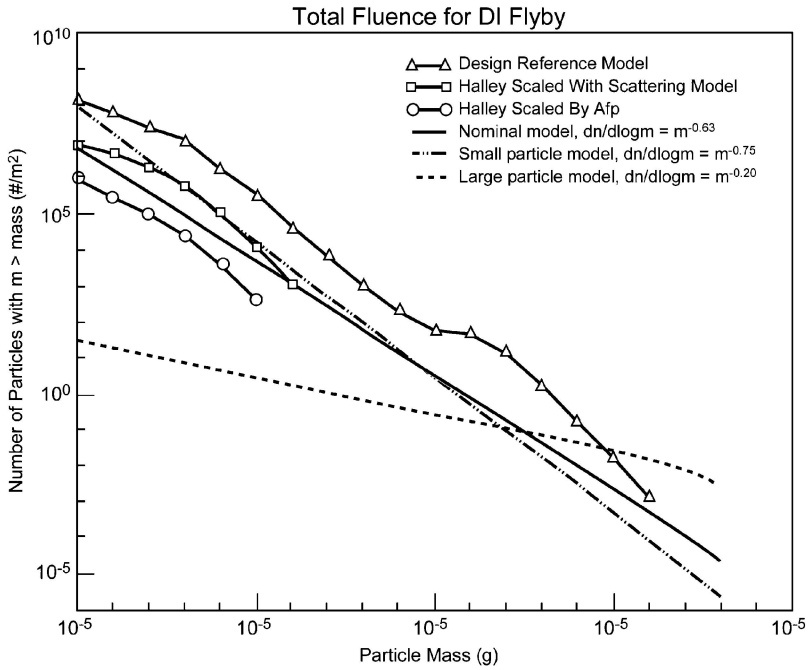

Figure 8. Estimated dust burden on the DI spacecraft during the Tempel 1 coma transit. Maximum ($m^{-0.76}$) and minimum ($m^{-0.63}$) small-particle-loaded particle mass distributions (PMDs) are consistent with the SED of Figure 5. Also shown is an example of a model that fit the mid-IR IRAS data well, but failed to reproduce the optical $Af\rho$ observation by more than an order of magnitude ($m^{-0.20}$). An independent measure of the number of small particles extant has been made using the *in situ* Halley encounter PMD of McDonnell *et al.* (1991), which is then scaled by the relative $Af\rho$ measures of Halley and Tempel 1 and forced to agree with the scattering model. There is good agreement between the two independent calculations. The range of relatively large-particle-dominated best-fit PMDs is consistent with the low dust albedo (<8%) and dust trail observed for the comet.

estimated burden of dust on the Deep Impact flyby spacecraft is $\sim$0.01 g m^{-2}, and on the impactor is $\sim$2 g m^{-2}.

For comparison, we include the results of Landgraf *et al.*'s (1999) radial model for the Stardust encounter with comet P/Wild 2. This model assumes a Halley size distribution (Lamy *et al.*, 1987), a constant particle density of 1 g cm^{-3}, coma structure driven by solar insolation and water and carbon monoxide ice sublimation, and a 70° phase angle, as expected for Stardust upon approach to comet P/Wild 2. We have scaled this model to DI at Tempel 1 using the relative activity ratio $Af\rho$ (Tempel 1)/$Af\rho$ (Wild 2) = (150/427), and the relative distance of closest approach of the two spacecraft, impact parameter (DI)/impact parameter (Stardust) = (500 km/100 km). It is interesting to note that while the predicted results for the radial models differ in their predictions for the fluence by a factor of a few in the medium mass ranges, the *total* mass integrated over all grain sizes

is quite similar for both, within 30% of 0.01 g m^{-2} at 500 km. The difference is that the two input dust model particle size distributions have very different large particle densities – most of the McDonnell Halley mass is in the abundant, large ($>10\ \mu$m) particles, while the Lamy Halley distribution has more smaller (1–5 μm) particles. The larger particles represent a bigger hazard to the DI spacecraft, however.

As an empirical check, we scaled the Tempel 1 model to the circumstances for the DS-1 flyby of P/Borrelly on September 22, 2001 ($Af\rho = 646$ cm at encounter, flyby distance = 2000 km). Our prediction for the number of dust particles detectable by perturbations of the spacecraft attitude control system, i.e. dust particles with mass $\geq$1 mg, was roughly 0.2 particles total burden, a factor of 10 lower than the DS-1 project dust model. For the actual flyby, no particles hits were detected, consistent with our predictions. Our prediction for the number of small ($\sim$1 μm) particles encountered was also within a factor of 2 of the number reported by Tsurutani *et al.* (2004) using the on-board 1 m dipole antenna to detect the transient electric field created by the expanding plasma clouds formed during dust particle hits. In a new study, the Tempel 1 dust model, when scaled to the circumstances of P/Wild 2 at the Stardust encounter ($Af\rho = 427$, flyby distance 230 km), was within a factor of 2 of the actual measured cumulative fluences (Tuzzolino *et al.*, 2004) over the mass range 10^{-11} to 10^{-2} g. The Stardust comparison is ultimately of greater use for the DI mission, as a finite number of particles were detected up to a mass of .01 g, whereas the DS-1 measurements only represent an upper limit for particles greater than 1 μg mass.

Encounter Expectations

Kind of Target

From our analysis, Tempel 1 appears to be an excellent target for the Deep Impact mission, as a "canonical" example of short-period cometary bodies. The gas emission from Tempel 1 is similar to other weak-emission-line comets according to Fink and Hicks (1996) and lies at the lower end of the range for "typical" composition comets (A'Hearn *et al.*, 1995), which includes all of the non-Jupiter family comets and one-third of the Jupiter family comets. From the work presented here, the dust emission from Tempel 1 seems entirely normal with respect to amount and kind compared to other short-period comets with many apparitions (Figure 6) like 2P/Encke, 55P/Tempel-Tuttle, and 73P/Schwassmann-Wachmann 3 (Lisse *et al.*, 2002). Similar to these comets, we also estimate that >90% of the dust is emitted by the comet into bound, stable solar system orbits, and eventually dissipates into the interplanetary dust cloud through perturbations due to dust–dust collisions and Poynting–Robertson drag (Burns *et al.*, 1979). Much of the heaviest bound dust is associated within a "trail," a stream of dust particles extending along the

orbital path of the comet, and is also typical of short-period comets on stable orbits (Sykes and Walker, 1992). The Tempel 1 dust trail was detected by IRAS in 1983 (Figure 4c).

Since the IRAS and optical light curves, when combined with respect to time from perihelion, seem to show the same behavior during the 1983, 1994 and 2000 apparitions (Figure 3), we conclude that the release of dust by Tempel 1 is repeatable from orbit to orbit within a factor of order unity. We can use this knowledge to predict the expected coma activity for the encounter phase of the DI mission in July 2005. Two days before perihelion, ($r_h = 1.51$ AU, $\Delta = 0.89$) $Af\rho$ (5500 Å) and $\varepsilon f\rho$ (12 μm) will be about 130 cm, Q_{dust} will be $\sim$250 kg s^{-1}, $Q_{OH} \sim 1.5 \times 10^{28}$ molecules s^{-1} and the Dust-to-Gas ratio will be $\sim$0.5. Given the broad appearance of the weak fan jet in the coma and an estimate of $\sim$8% active area on the surface (Groussin *et al.*, 2004), we surmise that emitted material is flowing from numerous active areas located across the nucleus surface. Thus, Tempel 1 should more closely resemble comet Wild 2, which had multiple weak sources, than comet Borrelly, which had a few very strong jets.

DI Coma Observations

The Deep Impact spacecraft will observe Tempel 1's coma before, during and after the encounter. Observations obtained during the approach will be used to determine the baseline characteristics of the coma, including its composition, structure and any temporal variations in these properties. Any features that are observed will be traced to their origin at the nucleus to help in understanding the link between the nucleus and the coma, a topic that is not well understood, even with several previous in situ comet missions. With constraints on the comet's baseline behavior, observations obtained during and after the impact will reveal changes in the coma that are produced by the impact. Two different instruments will be used to study the coma (Hampton *et al.*, 2005). The medium resolution imaging (MRI) camera, fitted with narrowband filters $\sim$70 Åwide, will obtain images of different gases (OH, CN and C_2) in the coma, as well as images of the dust at several different wavelengths. The high resolution imaging infrared spectrometer (HRI-IR) will measure the spectrum of the coma in the wavelength range 1.0–4.8 μm, at a resolving power $700 > R > 200$. Both instruments will provide the highest spatial resolution ever obtained on a cometary coma.

Narrowband imaging and optical spectroscopy, both discussed earlier, have shown that many different species (OH, CN, NH, and NH_2) exist in the coma of Tempel 1. Their parent species, H_2O, HCN, and NH_3 must exist as well. The Vega IKS spectrum of comet 1P/Halley 1986 (Combes *et al.*, 1988) and the ISO PHT-S spectrum of comet C/Hale-Bopp 1995 O1 (Lellouch *et al.*, 1998) represent by far the best knowledge of the neutral species we can expect to find in the cometary coma. The gaseous molecular species H_2O, CO, CO_2, CH_3OH, H_2CO (and possibly OCS) were detected from 2–5 μm in these spectra. As the Deep Impact spectrometer will

be observing Tempel 1 at higher spatial and spectral resolution and with much better sensitivity than were obtained at either Halley or Hale-Bopp, and since it is of "typical" composition, as were Halley (A'Hearn *et al.*, 1995) and Hale–Bopp (Schleicher, private communication), it is plausible to expect these species to appear in the coma of Tempel 1 as well. Simulations by Sunshine *et al.* (2005) indicate that we should detect H_2O at several wavelengths, CO_2 at 4.2 μm, two peaks of CO at 4.5 μm and possibly another at 2.15 μm. Emission lines in the 3.1–3.6 μm region due to the C–H aliphatic stretching mode will be obtained, mixed in with CH_3OH broad emission lines at 3.4 μm and H_2CO at 3.6 μm. However, as these simulations were based on observations of Oort-cloud comets, whereas Tempel 1 is a Jupiter-family comet with Kuiper belt origin, some differences in the observed chemistry might be expected that could be related to place of formation. Dust should be easily detectable in either case as scattered and themal continuum IR emission in the spectrum.

Using the multiple gas filters of the DI MRI camera, we expect to have a global overview of the coma with a spatial resolution of a few kilometers per pixel. With the images obtained, the spatial distribution of the majority gas species will be used to help in tracing the sources of the species, as well as providing measurements that can be used to study the photodissociation of their parent molecules (e.g. H_2O and CO). Dust jets will be imaged from the outer to the inner coma and down to their roots on the comet surface. Observations obtained with the Deep Impact infrared spectrometer will allow an accurate determination of the volatile production rates of the coma before and after impact. A large increase in observed CO production due to impact excavation is a likely possibility. The high spatial resolution available with the spectrometer (five times greater than with the MRI camera) also allows us to explore the near nucleus region that is unresolvable from the ground. This should allow DI to detect species with relatively short lifetimes, such as SO_2 and NH_3. These species have very weak emission lines but are located in a very clear region of the spectrum (4.0 and 2.3 μm, respectively) that favors their detection. The high spatial resolution will also allow us to compare the composition of the individual jets to each other and to the general coma composition.

The data return strategy (Klaasen *et al.*, 2005), constrains the observations that are possible, so between impact and the time the DI flyby enters shield mode (800 s after impact) only the infrared spectrometer will be used to study the gas coma. The main objective at this time will be to track changes in the composition of the coma and the potential appearance of new volatiles, and an off-nucleus scan will be performed for that purpose. Because the impact should expose fresh subsurface ices, we expect the coma to be enriched in highly volatile molecules such as CO and CO_2. From 44 min to 2.5 days after impact, after the impact science data has been telemetered to the ground, the lower constraints on data storage and transmission again allow us to observe the coma with the MRI narrowband filters as well as with the infrared spectrometer. During this phase, changes in the coma morphology and

composition will be monitored to study the longer-term effects of the impact as the comet returns to a steady-state condition. In particular, we will focus on any new jets to determine their number (one or more), locations (relative to the impact site), and structure (collimated or not). The MRI images will allow us to measure any enrichment in OH and/or carbon-bearing molecules after impact and to determine if the variations of composition in the coma are global or are restricted to the impact region. The production rates of H_2O, CO, CO_2, CH_3OH, H_2CO (and possibly other molecules) will be determined from the infrared spectrometer. The ultimate goal is to compare the production rates before and after impact, to study the effect of the impact on the gas coma and the relation between the coma and the nucleus. If the impact has no effect at all on the gas coma, which would be very surprising, it will still be very interesting, as it will oblige us to review our current view of comets.

Long-term Effects of the Impact on the Coma

Does the Deep Impact experiment effectively end 2.5 days after impact, when the flyby stops observing the comet? Given our derived estimate for the coma dust surface brightness, we can make a conservative estimate of how long the ejecta from the Deep Impact encounter will be detectable. (Note that this analysis ignores the possibility that a new, long-lived, active region will be created, which is a distinctly possible outcome. If a new source is created, this will only increase the duration of the impact-derived effects.)

We derive an estimate of the "impact duration" based on the time at which the spatial density of the impact ejecta has dropped to the level of the density of the nominal coma. The current best crater model predicts a crater some 100 m in diameter and 20 m deep. Assuming an ellipsoidal final crater, a bulk density for the nuclear material near the surface of 0.4 g cm^{-3}, a dust-to-gas ratio of 2, and $\sim$10% of the excavated material moving at speeds higher than the local escape velocity (Richardson, 2003, private communication), we can expect some $M_{\rm expl} = 2\times10^7$ kg of dust ejected into the coma due to the impact. Assuming that one-half of the crater material is ejected into a sold angle of $2/3\pi$ (Richardson, 2004, private communication; Schultz *et al.*, 2005), expanding at velocity $v_{\rm expl}$ with the same particle size distribution as the nominal coma dust, we have

$$n(r)_{\rm expl} = \frac{(1/2) \times M_{\rm expl}}{(2/9\pi(v_{\rm expl} \times t)^3)}$$

where t is the time since impact. Setting this quantity equal to the coma dust density from the comet's normal outgassing

$$n(r)_{\rm dust} = \frac{Q_{\rm dust}}{4\pi r^2 v_{\rm dust}}$$

we find that the time after impact when the ejecta shell is reduced to the density of the normal coma is given by

$$t_{\rm expl} = 9 \times \frac{M_{\rm expl}}{Q_{\rm dust}} \times \frac{v_{\rm dust}}{v_{\rm expl}}.$$

Clearly, the more dust that is ejected and the slower the ejection rate, the longer the time the impact perturbation is significant. We find an ejecta velocity of $v_{\rm expl} \sim 45\,{\rm m\,s^{-1}}$ by assuming all the kinetic energy of the impactor is converted into kinetic energy of the ejected dust (the recoil energy of the $\sim 10^{14}$ kg comet nucleus is negligible):

$$E_{\rm impactor} = 0.5 \times 350\,{\rm kg} \times (10\,{\rm km\,s^{-1}})^2 = 0.5 \times 2 \times 10^7\,{\rm kg} \times v_{\rm expl}^2.$$

where $v_{\rm expl} \gg v_{\rm escape} \sim 2\,{\rm m\,s^{-1}}$, as required for material ejected onto hyperbolic escape velocities into the coma. From the results of experimental cratering studies, Schultz *et al.* (2005) argue for a lower speed for the bulk of the ejecta, $\sim 10\,{\rm m\,s^{-1}}$, which is emitted late in the crater formation process, but still in the same order of magnitude as the velocity derived from the simplistic energy balance equation above.

Assuming a compromise average value of $v_{\rm dust} = 20\,{\rm m\,s^{-1}}$ and a normal coma dust emission rate of $Q_{\rm dust} = 250\,{\rm kg\,s^{-1}}$ (the average value from our modeling of the IRAS data), we find $t_{\rm expl} \sim 27$ days for the density equilibration time. The persistence of the Tempel 1 ejecta signal is due to the large amount of material thrown into the coma at very low speeds above the escape velocity from the impact. How does this compare to other timescales that are observed in the coma? It is short compared to the 115 days estimated time required to cross the observable coma (2×10^5 km; Figure 4) at $20\,{\rm m\,s^{-1}}$, and the $\sim$100 day lifetime of particles lofted into temporary, near-nucleus orbits (Scheeres and Mazari, 2000). It is long compared to the 5–10-day lifetimes of coma "shells" seen in other comets (e.g. Halley in 1986; Larson *et al.*, 1987; Hale-Bopp in April 1996; Lisse *et al.*, 1999). The 27-day timescale is also long compared to the $\sim$1-day timescale for the detection of the large, actively outgassing fragments emitted by comets C/Hyakutake 1996 B2 and C/1999 S4 (LINEAR).

If the pieces of ejected nucleus outgas rapidly, we will see a brighter ejecta structure of shorter duration, as the fragments disperse as they evaporate and accelerate under jet forces. Our estimate of how long the impact ejecta will be visible is also uncertain to $\sim$50% in the ratio of $v_{\rm dust}/Q_{\rm dust}$, and to a factor of a few in the ratio of $M_{\rm expl}/v_{\rm expl}$. Given these uncertainties, we believe a conservative range of $5 < t_{\rm expl} < 100$ days is best adopted for planning purposes. Observations of the progress of the ejecta shell through the coma should be designed using this time range.

To answer the question posed at the beginning of this section: The effects of the DI experiment will be observable for at least 5 days, and for as long as 100 days, after the time of the last DI flyby spacecraft observation. Extremely useful information

on the ejected particle sizes, compositions, and velocities will be obtained from observations of the progression of the ejecta through the coma, both from the DI flyby spacecraft and from ground-based telescopes. The role of other observing platforms will be critical at this point in time to understanding the nature of the coma and its origin in the material comprising the nucleus of the comet.

Conclusions

Previous observations of the gas emission from comet 9P/Tempel 1 have found its composition to be at the lower end of the range of "typical" comets in carbon-chain molecules relative to water. As the gas emission behavior seems relatively stable from apparition to apparition, we expect a total outgassing rate $\sim 1 \times 10^{28}$ molecules per second and a gas composition of $\log(\mathrm{CN/OH}) \sim -2.83$, $\log(\mathrm{C_2/OH}) \sim -2.90$, $\log(\mathrm{C_3/OH}) \sim -4.06$, and $\log(\mathrm{NH/OH}) \sim -2.55$ at encounter.

The dust emission from Tempel 1 is very similar to that seen from other short-period comets that have had a large number of perihelion passages. At encounter, the comet will be emitting $\sim$250 kg/s of dust into the coma, with the majority of the particle surface area and mass in particles with radius $\mathbf{a} > 20\ \mu$m. The pre-encounter Dust-to-Gas rated will be $\sim$0.5.

The long-term activity of the comet, as depicted in the continuum lightcurve, shows a peak in the activity around 60 days before perihelion. Furthermore, the onset of activity is much steeper than the decrease after the peak, causing an additional asymmetry around the peak itself. This behavior is likely due to the competing effects of seasonal variations and the increasing solar irradiance as the nucleus gets closer to the sun. The seasonal effect produces the early peak, while the increased amount of sunlight at perihelion causes the overall emission to be higher than it was before the peak. It is likely that the emission from the observed jet is related to the seasonal effect and is contributing to the increased activity level. This would indicate that the sun is at its highest elevation, as seen from the source, at -60 days. Although no jets have been detected at other times, this may simply reflect the fact that there are only a limited number of high-quality, high-resolution images available.

The presence of a jet indicates that there is one or more isolated sources on the nucleus, even though the coma generally has an isotropic appearance. This result is consistent with thermophysical models of the nucleus surface (Groussin *et al.*, 2004) that indicate only 8% of the surface area is active. This small active fraction further hints that the isotropic component of the coma may be produced by a number of small, diffuse jets that mimic an isotropic shape (e.g., comet Wild 2, Sekanina *et al.*, 2004).

The nucleus will be detectable against the coma background from DI at $\sim$9 days before impact in July 2005. A total dust fluence of $\sim$2 g at 10 km s^{-1} per m^2 of projected spacecraft surface area will be experienced by the DI impactor, and

0.02 g per m^2 by the DI flyby (with minimum approach distance of 500 km to the nucleus). The ejecta should be detectable against the coma background for some time after the impact. From simple arguments, we estimate the time for the ejecta to fade into the existing coma will be as little as 5 days and as much as 100 days after impact.

Acknowledgments

The authors wish to thank A. Cochran, P. Feldman, and R. Walker for kindly supplying their archival observations of Tempel 1, Stephanie McLaughlin for helping to produce the long term lightcurves, and S. Kido for mastering the figure graphics. Comments by A. Cochran and an anonymous reviewer were very helpful in improving the manuscript. In pursuing this work, the authors were partially supported by the Deep Impact project, and Planetary Astronomy Grants NAG5-9006 and NAG-11468.

References

A'Hearn, M. F., Schleicher, D. G., Feldman, P. D., Millis, R. L., and Thompson, D. T.: 1984, *Astron. J.* **89**, 579.

A'Hearn, M. F., Millis, R. L., Schleicher, D. G., Osip, D. J., and Birch, P. V.: 1995, *Icarus* **118**, 223.

Belton, M. J. S., Meech, K. J., A'Hearn, M. F., Groussin, O., McFadden, L. A., Lisse, C. M., *et al.*: 2005, *Space Sci. Rev.*, *ibid.*

Bockelee-Morvan, D., Crovisier, J., Mumma, M. J., and Weaver, H. A.: 2005, in Festou, M., Keller, U., and Weaver, H. (eds.), *Comets II*, University of Arizona Press, Tucson.

Boice, D. and Huebner, W.: 2005, in Festou, M., Keller, U., and Weaver, H. (eds.), *Comets II*, University of Arizona Press, Tucson.

Burns, J. A., Lamy, P. L., and Soter, S.: 1979, *Icarus* **40**, 1.

Campins, H., Walker, R. G., and Lien, D. J.: 1990, *Icarus* **86**, 228.

Cochran, A. L., Barker, E. S., Ramseyer, T. F., and Storrs, A. D.: 1992, *Icarus* **98**, 151.

Combes, M., *et al.*: 1988, *Icarus* **76**, 404.

Combi, M. R., Harris, W. R., and Smyth, W. H.: 2005, in Festou, M., Keller, U., and Weaver, H. (eds.), *Comets II*, University of Arizona Press, Tucson.

Crifo, J. F., Fulle, K. M., and Szego: 2005, in Festou, M., Keller, U., and Weaver, H. (eds.), *Comets II*, University of Arizona Press, Tucson.

Farnham, T. L. and Schleicher, D. G.: 2005, *Icarus* **173**, 533.

Farnham, T. L., Schleicher, D. G., and A'Hearn, M. F.: 2000, *Icarus* **147**, 180.

Fernandez, Y. R., Lisse, C. M., Ulrich, K. H., Peschke, S. B., Weaver, H. A., A'Hearn, M. F., *et al.*: 2000, *Icarus* **147**, 145.

Fernandez, Y. R., Meech, K. J., Lisse, C. M., A'Hearn, M. F., Pittichova, J., and Belton, M. J. S.: 2003, *Icarus* **164**, 481.

Feldman, P. and Festou, M.: 1991, in Harris, A. W. and Bowell, E. (eds.), *Proceedings of ACM 1991 on IUE Observations of Periodic Comets Tempel 2, Kopff, and Tempel 1*, Lunar and Planetary Institute, Houston, pp. 171.

Feldman, P., Combi, M., and Cochran, A.: 2005, in Festou, M., Keller, U., and Weaver, H. (eds.), *Comets II*, University of Arizona Press, Tucson.

Fink, U. and Combi, M. R.: 2004, *Plan. Space Sci.* **52**, 573.
Fink, U. and Hicks, M.: 1996, *ApJ* **459**, 729.
Finson, M. L. and Probstein, R. F.: 1968, *Astron. J.* **154**, 327.
Groussin, O., Lisse, C. M., A'Hearn, M. F., Belton, M. J., Fernandez, Y. R., van Cleve, J. E., *et al.*: 2004, Thermal Properties of Deep Impact Target Comet 9P/Tempel 1, COSPAR Meeting 35, abstract B1.1 002204.
Hampton, D. L., Baer, J. W., Huisjen, M. A., Varner, C. C., Delamere, A., Wellnitz, D. D., *et al.*: 2005, *Space Sci. Rev., ibid.*
Harker, D., Woodward, C. E., Wooden, D. H., Witteborn, F. C., and Meyer, A. W.: 1999, *Astron. J.* **118**, 1423.
Jessberger, E. K., Christofordis, A., and Kissel, J.: 1988, *Nature* **322**, 691.
Jessberger, E. K. and Kissel, J.: 1991, in Newburn, Neugebauer, and Rahe (eds.), *Comets in the Post-Halley Era*, Kluwer Academic Publishers, Dordrecht, pp. 1075.
Klaasen, K. P., Carcich, B., Carcich, G., Grayzeck, E. J., and McLaughlin, S.: 2005, *Space Sci. Rev., ibid.*
Krasnopolsky, V. A., Moroz, V. I., Krysko, A. A., Tkachuk, A. Y., and Moreels, G.: 1987, *Astron. Astrophys.* **187**, 707.
Lamy, P. L., Grün, E., and Perrin, J. M.: 1987, *Astron. Astrophys.* **187**, 767.
Landgraf, M., Müller, M., and Grün, E.: 1999, *Plan. Space Sci.* **47**, 1029.
Larson, S., Sekanina, Z., Levy, D., Tapia, S., and Senay, M.: 1987, *Astron. Astrophys.* **187**, 639.
Lebofsky, L. A. and Spencer, J. R.: 1989, *Asteroids II*, University of Arizona Press, Tucson, pp. 128.
Lellouch, E., Crovisier, J., Lim, T., Bockelee-Morvan, D., Leech, K., Hanner, M. S., *et al.*: 1998, *Astron. Astrophys.* **339**, L9.
Lien, D. J.: 1990, *Astron. J.* **355**, 680.
Lisse, C. M., Freudenreich, H. T., Hauser, M. G., Kelsall, T., Moseley, S. H., Reach, W. T., *et al.*: 1994, *ApJ* **432**, L71.
Lisse, C. M., A'Hearn, M. F., Hauser, M. G., Kelsall, T., Lien, D. J., Moseley, S. H., *et al.*: 1998, *ApJ* **496**, 971.
Lisse, C. M., *et al.*: 1999, *Earth, Moon, Planets* **78**(1/3), 251.
Lisse, C. M., Fernandez, Y. R., A'Hearn, M. F., and Peschke, S. B.: 2002, in Green, S. F., Williams, I. P., McDonnell, J. A. M. (eds.), *COSPAR Colloquia Series Vol. 15, Dust in the Solar System and Other Planetary Systems*, pp. 259.
Lisse, C. M., A'Hearn, M. F., Fernandez, Y. R., Gruen, E., Kaufl, H. U., Kostiuk, T., *et al.*: 2004, *Icarus* **171**, 444.
Lynch, D. K., *et al.*: 1995, *Icarus* **114**, 197.
Marsden, B. G. and Williams, G. V.: 2003, *Catalogue of Cometary Orbits*, XVth edn. Central Bureau for Astronomical Telegrams and Minot Planet Center, Cambridge, Massachusetts.
Mason, C. G., Gehrz, R. D., Ney, E. P., Williams, D. M., and Woodward, C. E.: 1998. *Astron. J.* **507**, 398.
McDonnell, J. A. M., Lamy, P. L., and Pankiewicz, G. S.: 1991, in Newburn, Neugebauer, and Rahe (eds.), *Comets in the Post-Halley Era (Bamberg Meeting Proceedings)*, Kluwer Academic Publishers, Dordrecht, pp. 1043.
Meech, K. J., A'Hearn, M. F., Lisse, C. M., Weaver, H. A., and Biver, N.: 2005, *Space Sci. Rev.*, *ibid.*
Ney, E. P. and Merrill, K. M.: 1976, *Science* **194**, 1051.
Osip, D. J., Schleicher, D. J., and Millis, R. L.: 1992, *Icarus* **98**, 115.
Reach, W. T., *et al.*: 1999, *Icarus* **148**, 80.
Reach, W. T., Sykes, M. V., Lien, D., and Davies, J. K.: 2000, *Icarus* **148**, 80.
Scheeres, D. J. and Mazari, F.: 2000, *Astron. Astrophys.* **356**, 747.
Schleicher, D. G. and Farnham, T.: 2005, in Festou, M., Keller, U., and Weaver, H (eds.), *Comets II*, University of Arizona Press, Tucson.

Schultz, P. H., Ernst, C. M., and Anderson, J. L. B.: 2005, *Space Sci. Rev.*, *ibid.*
Sekanina, Z.: 1981, *Astron. J.* **86**, 1741.
Sekanina, Z., Brownlee, D. E., Economou, T. E., Tuzzolini, A. J., and Green, S. F.: 2004, *Science* **304**, 1769.
Storrs, A. D., Cochran, A. L., and Barker, E. S.: 1992, *Icarus* **98**, 163.
Sunshine, J. M., A'Hearn, M. F., Groussin, O., McFadden, L., Klaasen, K. P., Schultz, P. H., *et al.*: 2005, *Space Sci. Rev.*, *ibid.*
Sykes, M. V., Lien, D. J., and Walker, R. G.: 1990, *Icarus* **86**, 236.
Sykes, M. V. and Walker, R. G.: 1992, *Icarus* **95**, 180.
Tokunaga, A. T., Hanner, M. S., Veeder, G. J., and A'Hearn, M. F.: 1984, *Astron. J.* **89**, 162.
Tsurutani, B. T.: 2004, *Icarus* **167**, 89.
Tuzzolino, A. J., *et al*., 2004, *Science* **304**, 1776.
Yeomans, D. K., Giorgini, J. D., and Chesley, S. R.: 2005, *Space Sci. Rev.*, *ibid.*